NASA Technical Memorandum 78782

(NASA-TM-78782) DUST ADHESION ON VIKING LANDER CAMERA WINDOW (NASA) 34 p HC A03/MF A01 CSCL 14E

N78-33407

Unclas

G3/35 33839

DUST ADHESION ON VIKING LANDER CAMERA WINDOW

JAG J. SINGH

SEPTEMBER 1978

NASA

National Aeronautics and Space Administration

Langley Research Center
Hampton, Virginia 23665

DUST ADHESION ON VIKING LANDER

CAMERA WINDOWS

By Jag J. Singh
Langley Research Center

ABSTRACT

Extensive studies of dust impingement on a duplicate Viking Lander camera window had indicated the possibility of window obscuration after several "days" of exposure even at low dust concentration levels. It was expected that the problem would be magnified considerably if the 0.040-inch clearance between the camera housing and the post was not closed. As a result of these studies, the following corrective measures had been recommended.

1. The clearance between the housing surface and the camera post should be eliminated by using an appropriately designed plastic "skirt."

2. The three horizontal ledges below the window inside the cavity act as bases for pile-up of dust that slides down the window surface. They should be replaced by a single inclined plane down which the dust will slide and fall out on the ground.

3. Adhered dust on the window surface can be removed by high pressure CO_2 jets directed down against the window. The amount of CO_2 gas needed for the entire mission can be carried in a 3½-inch-diameter sphere equipped with a remotely programable valve. These measures were incorporated in the design of the lander camera system. The continued high quality of photographs transmitted from the Viking spacecraft several months after landing attests to their effectiveness.

INTRODUCTION

The National Aeronautics and Space Administration launched two spacecraft in 1975 and soft landed them on the surface of Mars. The lander instruments had been designed to provide detailed information about the organic and inorganic composition of Martian soil and included three meteorology sensors, a seismometer, two facsimile cameras and a specially designed collector head to collect soil specimen for measuring surface properties. The cameras would serve as the eyes for the Viking investigators to view the Martian topography and surface structure in color and stereovision. The great importance of these cameras to the success of Viking mission made it necessary to take all precautionary measures to ensure their unhindered performance under the prevailing Martian conditions.

Martian surface is dust covered and wind speeds as high as 60 m/sec are not uncommon (refs. 1, 2). Mariner 9 experimenters had reported observing frequent dust storms. These storms are highly convective and carry dust rapidly to heights of 15 → 20 km (ref. 3). These frequent dust storms will result in significant amounts of dust being projected against the camera windows. Some of this dust may adhere to the window surface. The presence of dust particles on the window surfaces can affect the transmission of light through them. The dust particles will also scatter light. The scattered light will have the general effect of reducing the contrast in the photographs taken through such windows.

When dust particles come in contact with glass surfaces, strong attractive forces come into play which may result in their adhesion. (See Appendix 1 for a discussion of the theory of particle adhesion on plane substrates.) Calculations of dry dust adhesion on quartz substrates indicate that Van der Waal's forces will lead to adhesion of all particles that meet the following criteria:

$$V_{\perp} < \frac{30}{d} \text{ centimeters per second} \qquad (1)$$

where $V_{\perp}$ = initial normal velocity component of the dust particles
and d = particle size in micrometers

Clearly, the neutral particles can adhere only in the cases when they are small in size and are moving slowly. (See Appendix 2 for more details.) But, the presence of high wind velocities and the resultant electrification on Mars bring in electrostatic forces which can lead to considerable enhancement in dust adhesive forces. Additionally, the impact of sand particles may charge the glass window and complicate the dust sticking phenomenon.

In view of the various uncertainties - such as the degree of dust electrification, window charge by friction/impact and the chemical composition of sand/dust particles involved - it was not possible to make a reliable calculation of the anticipated dust adhesion problem. It was therefore decided to make an experimental assessment of the Viking window obscuration problem. Briefly, the experimental plan involved exposing the test windows to various levels of dust impingement and taking photographs of a calibration object through these exposed windows. An examination of the calibration grid photographs is expected to show the effects of changes in the transmissibility of light resulting from the presence of dust on the exposed windows. The results of these experiments are described below.

Experimental Procedure

In order to simulate the Martian environmental conditions, the following guidelines were established.

Dust concentration.-Dust concentration corresponding to visibility distances ranging from (1 km → 1 m) were selected to represent the extreme

Martian storm conditions. These concentrations range from $(10^{-9} \rightarrow 10^{-6})$ gm/cc. These should be compared with Mars Engineering Model (Revised) values of $\simeq 2 \times 10^{-7}$ gm/cc (dust) and $\simeq 2 \times 10^{-7}$ gm/cc (sand) at camera window heights in an average storm (typical velocity of 10 meters/sec). (Ref. 4)

Dust size distribution.- From nominal lunar soil specimen(*) kept at Langley, particles of diameter equal to or less than 105 μm were separated. Majority of dust/sand particles in the top loose layer of Martian soil are expected to fall in this size range (ref. 5). Actually it is only the smaller particles (diameter ≤ 10 μm) that are likely to adhere to the window surfaces. However, particles of size greater than 10 μm were included in the mixture because they make the wind burden more representative of the conditions within 2 meters of the surface during an average Martian storm. Consequently, any frictional charging of dust particles that might occur in a Martian storm would also occur in the proposed experimental study. The presence of electrical charge on the dust particles is expected to play an important role in their adhesion to window surfaces.

Wind Speed.- Wind velocities ranging from dust particles terminal velocities to average storm particle velocities (1 → 1000 cm/sec) were selected to be representative of the normal Martian wind velocity spectrum.

Water content.- It has variously been surmised that all precipitable moisture in Martian atmosphere will produce $\simeq 20$ μm/cm^2 thick water layer. The weight of Martian atmosphere has been estimated to be about 16 gm/cm^2. These figures give water content of about 100 ppm (weight) if one assumes that water vapor is distributed uniformly through the Martian atmosphere. However, if one assumes that most of the water vapor is confined to the lower atmosphere (≤ 1 km), one obtains a figure of about (200 - 300) ppm (weight).

Martian atmospheric pressure.- A range of values of (4 → 10) millibars was selected to encompass the then current state of information about the Martian atmosphere. (Ref. 4)

These guidelines are summarized in Table 1. Also shown in this table are the experimentally attained values of these parameters in parts I and II of this study. Actually, part I was directed more towards establishing the experimental procedure to achieve the selected ranges of various parameters than obtaining the final data. As can be seen from the table, two critical parameters - dust concentration and humidity - had not yet been adjusted to correspond to the selected ranges for them. However, certain conclusions - such as the effect of geometrical features of the window cavity and the effect of the particle speed on the adhesion phenomenon - could properly be drawn on the basis of this part of the study.

(*) The composition of, and the particle size distribution in, nominal lunar soil were assumed to be similar to the Martian soil (ref. 4).

Figure 1 shows a schematic diagram of the 5' x 5' vacuum chamber that was used to simulate the Martian environment. An internal aluminum chamber was installed to confine the dust to the experimental region. The two chambers (chamber #1 and #2 in the figure) were pumped down separately. The pressure gage and the hygrometer were located in the outer chamber. Figure 2 shows a photograph of the interior of the 5' x 5' chamber. A CO_2 jet ($\simeq 150$ cm/sec) was directed into a wooden hopper which held about 1 pound of dry(*) lunar nominal soil (particle size $\lessapprox$ 105 μm). The resultant dust storm inside the hopper was then guided through appropriate rubber tubes to adjust the ex-flow rate through the tubes. The ensuing dust-laden gas was allowed to strike against duplicate(**) camera housing window. In order to determine the dust concentration, the camera housing assembly was replaced by a plastic bag whose opening area was equal to the window area. The dust collected in the bag after a 15-minute flow was measured and the dust concentration calculated. Assuming that the dust concentration is determined by the stirring CO_2 gas jet speed and that the ex-flow rate of the dust-laden gas is inversely proportional to the exit tube area, the exit gas flow rate can be controlled. In this manner, by choice of three different size rubber tubes through which the dust-laden gas exited, wind velocities of 1.5 cm/sec, 15 cm/sec, and 60 cm/sec were obtained keeping a constant dust concentration. In order to study the effects of dust adhered to the window on light transmission through it, a film transparency with several increasingly finely divided grids impressed on it was mounted behind the window. The transparency, which served as the object, was illuminated with a light source located inside the camera housing and photographed through the test window before and after dust impingement on it. All photographs were taken <u>in situ</u>, without disturbing the environment or the system. The photographs were taken with a camera, located outside the chamber, through a test chamber window protected from dust exposure during the test.

The results of constant concentration dust bombardment for 15-minute periods at three different speeds are shown in figures 3 → 5. Fifteen-minute exposures were selected because the present Viking plans called for the use of lander cameras for 15 minutes per day. Thus a 15-minute exposure to dust impingement is equivalent to "1-day" exposure on the Mars. Also shown in these figures are the results of a CO_2 jet being directly directed against dust-covered window. Several 1-second CO_2 jet blow-offs at 100 cc/sec at 40 psi were needed to clear up a dust covered window. An examination of the window cavity after each of these runs showed that dust had accumulated on the horizontal ledges below the window. This deposited dust, when distributed by the incident dust-laden gas stream, served as an additional source of impingement dust.

(*) The soil was dried by heating it for 2-4 hours at 200°C in vacuum and then flooded with dry CO_2 before transfer to the hopper.
(**) An exact duplicate of the upper part of the camera housing assembly with appropriately coated quartz window was used.

In order to determine the effects of general dust settlement on camera window, the dust hopper shown in figures 1 and 2 was removed. A thin layer of dry lunar soil ($\leq$ 105 μm) was spread on the floor of the inner chamber and dry CO_2 jets (> 100 cm/sec) were directed against the inner chamber walls. This procedure was expected to lead to some fine dust suspension in the inner chamber. The gas jets were fired for a short time to raise the chamber pressure to $\leq$ 20 mm (Hg). There was a 5-minute interval between consecutive CO_2 gas jet firings. After a total run time of 35 minutes, it was determined that a horizontal surface collected $\simeq 2 \times 10^{-4}$ gm/cm^2 (which corresponds to an average dust concentration of 1.0×10^{-7} gm/cc). During this time, there was determined to be no visible change in the transmissibility of the camera window. (See figure 6.) The vertical test window also, presumably, had a dust deposition $\simeq 2 \times 10^{-5}$ gm/cm^2 (assuming no gravity-induced slippage).(*) Figure 7 shows a magnified view of the camera window, before and after the run. A thin layer of deposited dust can clearly be seen on the window.

It has been assumed that the dust particles will be reaching the window only when the camera post is not in front of the window, i.e., only 15 minute/day. However, the presence of 0.040-inch clearance between the post and the housing surface will permit dust to arrive at the window all the time, thereby magnifying the probability of window obscuration.

In the second part of the study, the two important parameters which had not been properly simulated in the first part had been reduced to their accepted range of values. Figure 8(a) shows a schematic diagram of the experimental arrangement used in this part of the study. Figure 8(b) shows a photograph of the interior of the test chamber. Dry, lunar nominal soil (particle size $\leq$ 105 μm) was stirred by a variable speed rocker and forced through a narrow sieve. This dust holder "assembly" was mounted at the top of a 12" x 12" x 12" aluminum "dust storm" box, which had two high speed CO_2 gas jets ($\simeq$120 cm/sec at 2500 cc/channel of CO_2 gas flow) crossing it across the falling dust. The CO_2 jets carried some of this dust in suspension and thus simulated the dust laden Martian atmosphere in channels 2 and 3 (see figure 8(a)). The amounts of dust collected in channels 2 and 3 were measured for various combinations of the rocker speed and the dust entraining in either channel based on the measured value of the dust collected in the other channel. This arrangement permitted a controllable dust concentration in the range $1.9 \times 10^{-7} \rightarrow 6.3 \times 10^{-6}$ gm/cc (see Table I for range of dust concentration values on Mars). The moisture content inside the test chamber was kept minimal by cooling the 5' x 5' chamber walls with liquid nitrogen. The measured values of the gas temperature ranged from -20°F at the center of the chamber (i.e., adjacent to the camera housing to -310°F at the chamber walls. The moisture content of the CO_2 gas ($\leq$ 100 ppm) alone

---

(*) Assuming isotropic dust concentration and velocity distribution.

determined the final water vapor pressure in the test chamber. Thus, using the present experimental apparatus, it had been possible to simulate the dust concentration as well as the low moisture content of the Martian atmosphere.

It should be pointed out that the velocity of the dust-laden CO_2 gas striking against the camera window can be controlled by controlling the speed of the CO_2 jets entering the "dust storm" box. However, the first part of the study had confirmed the calculations that the dust adhesion is more pronounced at lower dust particle speeds than at higher speeds (see Appendix 2). Hence, most of the measurement in this part of the study were devoted to low speed ($\simeq$4 cm/sec) dust particles striking against the camera window.

EXPERIMENTAL RESULTS

Data obtained in the first part of the study indicated that dust adheres easily to the quartz window and that dust adhesion is more marked at lower speeds. For example, a comparison of figures 3-5 clearly shows that the window obscuration at wind speed of 1.5 cm/sec is more marked than at 60 cm/sec for the same dust concentration. Figures 6 and 7 show that general settlement of dust, infiltrating inside the cavity through the 0.04" clearance between the housing surface and the post, can also cause some loss in window light transmission.

In view of the results shown in figures 3-5, the second half of the study was confined to low speed ($\simeq$4 cm/sec) dust particles striking against the glass window. The dust adhesion phenomena was studied at several levels of dust concentration in order to determine the validity of normalizing the data taken at higher concentration to that at lower dust concentration. For example, figures 9 and 10 show a comparison of dust deposited at three levels of dust concentration. The second photograph in figure 9, taken after a 135-minute exposure at 1.9×10^{-7} gm/cc @ 4 cm/sec, should be compared with the third photograph in the same figure taken after 15-minute exposure at 1.6×10^{-6} gm/cc @ 4 cm/sec. Similarly, the second photograph in figure 10 (taken after a 60-minute exposure at 1.6×10^{-6} gm/cc @ 4 cm/sec should compare with the third photograph (taken after a 15-minute exposure at 6.3×10^{-6} gm/cc @ 4 cm/sec). Figures 9 and 10 clearly show that at these low levels of dust concentration there is no fundamental difference between the adhesion processes even when the dust concentration changes by almost a factor of 35!

Figure 11 shows a comparison between a 15-minute exposure at 6.3×10^{-6} gm/cc @ 4 cm/sec and a 15-minute exposure at 3×10^{-6} gm/cc @ 8 cm/sec. The two photographs in figure 11 are almost identical, indicating that the dust flux ($\equiv$ dust concentration x dust velocity) is the more relevant parameter in the low dust speed and the low dust concentration regime. From figures 9-11, it would appear that data normalization in terms of dust concentration and dust speed is reasonably justifiable in the low dust concentration and low speed regions. Figure 12 shows the effects of several window exposure times at 4.5×10^{-6} gm/cc @ 4 cm/sec. Clearly an exposure of 30 → 60 minutes duration at 4.5×10^{-6} gm/cc @ 4 cm/sec causes a distinct loss in light transmission through the window.

Whereas we did not know the exact dust concentration at Mars - it can range from $10^{-9} \rightarrow 10^{-6}$ gm/cc - it did appear that even at very low dust concentration at low speeds, and exposure of 1-2 hours (several "equivalent days") could cause a measurable loss in the transmissibility of the camera window. On this basis, it appeared to be necessary to take measures to counteract the dust deposition. One such measure, which had been recommended in the earlier formulation of the problem, involved the use of a CO_2 jet under high pressure. This measure was suggested by the facts that CO_2 gas is available onboard the lander and that CO_2 would not contaminate the Martian atmosphere. Figure 13 shows the results of a single 0.1 sec CO_2 jet at 1000 psi against the window which had been exposed for 60 minutes at 4.5×10^{-6} gm/cc @ 4 cm/sec. Clearly photograph no. 3 in this figure, which was taken after the 0.1 second CO_2 jet blow-off, is as clear as photograph no. 1 which was taken before any dust deposition. Under the present experimental conditions, a single CO_2 jet uses 450 cc of gas at STP. At this rate, about 20 cubic inches of CO_2 (liquid phase) would be required to provide one jet blow-off/day for 3 months for the two lander cameras. In addition to CO_2, helium gas was also tested as the blow-off jet gas. As expected from theoretical considerations, a 0.1 second CO_2 gas jet at 1000 psi was much more effective in removing the adhered dust than the helium jet under the same conditions. Helium gas will have to be used at a much higher pressure - probably several thousand psi - to be as effective as CO_2 gas at 1000 psi. (The 0.1 second jet duration, as well as the 1000 psi level, was dictated by the mechanical characteristics of the solenoid valve used in these studies.)

CONCLUSIONS

As a result of the foregoing study, the following conclusions had been drawn.

1. At low speeds, even at low dust concentration normally expected at Mars, dust adhesion on camera windows could cause light obscuration after several "days" of equivalent exposure. This problem would be increased considerably if the 0.040" clearance between the camera housing and the post is not eliminated.

2. The high concentration data in part I had shown that the three horizontal ledges at the bottom of the window inside the cavity act as bases for pile-up of dust that slides down the window surface. They should be replaced by a single inclined plane down which the dust would slide and fall out on the ground.

3. Adhered dust can be removed by high pressure, high speed jets of CO_2 gas directed against the window surface. The amount of CO_2 gas needed for the entire mission could be carried in a 3½-inch-diameter sphere equipped with a programable valve.

All the necessary modifications/additions were incorporated in the design of the lander camera systems. The continued high quality of the photographs transmitted from the Viking lander, several months after successfully landing on Mars, attests to the effectiveness of the remedial procedures that had been prescribed after the study described herein.

REFERENCES

1. S. Glasstone: "The Book of Mars." NASA SP-179, 1968.

2. G. S. Golitsyn: Icarus. 18, 113, 1973.

3. C. B. Leovy; G. A. Briggs; A. T. Young; B. A. Smith; J. B. Pollack; E. N. Shipley; and R. L. Wilday: "Mariner-9 Television Experiment: Progress Report on Studies of the Mars Atmosphere." Icarus. 17, 373, 1972. (Also see, Hess: Plant. Space Sci., 21, 1549, 1973)

4. Mars Engineering Model, Viking 75 Project. Prepared by NASA-LRC, 1970.

5. T. D. Rusert; J. Gliozzi; G. Romine; and P. Fennessey: Martin Marietta Corporation Report # TR-372-2-0, Nov. 1971.

6. R. S. Bradley: Phil. Mag. 13, 853, 1932. Trans. Faraday Soc. 32, 1088, 1936.

7. H. C. Hamaker: Physics 4, 1058, 1937.

8. E. M. Lifshitz: Soviet Physics, JETP 2, 73, 1956.

9. H. Crupp: Advances in Colloid and Interface Science, 1, 111, 1967.

10. H. F. Eden and B. Vonnegut: Science, 180, 962, 1973.

Table I.- Summary of the Experimental Conditions.

Parameters	Recommended Range	Values Obtained in the First Part of the Study	Values Obtained in the Second Part of the Study
Dust concentration	$10^{-9} \rightarrow 10^{-6}$ gm/cc	$(4 \rightarrow 5)\ 10^{-4}$ gm/cc	$(1.9 \times 10^{-7} \rightarrow 6.3 \times 10^{-6})$ gm/cc
	(Viking revised value at 1 meter altitude $\simeq 2 \times 10^{-7}$ gm/cc)		
Dust particle size	Lunar nominal	$\lessapprox$ 105μm (Lunar nominal)	$\lessapprox$ 105 μm (Lunar nominal)
Wind speed(*)	$(1 \rightarrow 1000)$ cm/sec	$(1.5 \rightarrow 60)$ cm/sec	$(4 \rightarrow 8)$ cm/sec
Water content	$\lessapprox$ 300 ppm (weight)	$(3500 \rightarrow 120{,}000)$ ppm	< 300 ppm (weight)

(*) First part of the study had shown that the dust adhesion problem is more pronounced at lower speeds, as expected. Hence the second part of the study was confined to low speeds.

APPENDIX 1

PARTICLE ADHESION THEORY

An important factor in the adhesion of dust particles on insulating surfaces is the type (or types) of interaction that occurs between them. Broadly speaking, there are three types of interactions that should be considered:

1. "Long" range attractive forces (Van der Waal's and electrostatic forces)

2. "Short" range attractive forces (various types of chemical bonds, including hydrogen bonds)

3. Attractive "molecular" forces resulting from mutual dissociation and alloying at the interface when high velocity particles strike against the substrate.

Interactions of type 3 were not considered in the present study, since they usually involve larger size and higher velocity particles which often lead to substrate erosion. (This type of interaction constitutes a different problem.) Interactions of the type 2 were also left out of consideration because the primary chemical bonds at the surfaces of the still-separated adherents will tend to become saturated by the contaminating substances, and thus be no longer available for chemical interactions with the other adherent. Furthermore, the probability of strong chemical bonds between insulating surfaces is very small. This leaves us, mainly, with the consideration of the type 1 attractive forces. We shall take up a discussion of Van der Waal's forces first.

Van der Waal's Forces

Two approaches to the calculation of Van der Waal's attractive forces between the solids will be discussed.

1. The microscopic theory which assumes the additivity of interactions between all pairs of individual atoms or molecules of the adherent bodies. This approach has certain drawbacks: It does not account for correlation of charge carrier motion in the two solids and also disregards the formation of new types of molecules at the contacting surfaces. A brief exposition of this theory follows:

The interaction potential between two nonpolar molecules or atoms can be written as follows:

$$U(r) = -\frac{\lambda}{r^6} + \frac{\mu}{r^{12}} \tag{1}$$

where λ and μ are the well-known Lennard-Jones force constants.

By integrating the attractive force between a pair of molecules over all molecules of adherents 1 and 2,

$$U_{12} = \lambda N_1 N_2 \iint \frac{d\tau_1 \, d\tau_2}{r^6} \tag{2}$$

Bradley (ref. 6) and Hamaker (ref. 7), calculated the attractive force between two identical solid spheres and obtained the following type of expression.

$$F_{12} = \left(\frac{\pi^2 \lambda N^2}{24 Z_o^2}\right)\left(\frac{d_1 d_2}{d_1 + d_2}\right) \tag{3}$$

where N = number molecules/cc

Z_o = separation between the two spheres when the adhesive force was maximum

$\simeq (4 - 5)$ Å

d_1 and d_2 are the diameters of the two interacting spheres.

The constant $\left(\frac{\pi^2 \lambda N^2}{24 Z_o^2} = \frac{A}{24 Z_o^2}\right)$ in cgs system was calculated to be 212 for for two quartz spheres, i.e.,

$$F_{12} = 212 \left(\frac{d_1 d_2}{d_1 + d_2}\right) \text{ dynes} \tag{4}$$

when d_1 and d_2 are expressed in units of centimeters.

Equation (3) reduces to the form:

$$F_{12} = Ad/24\ Z_o^2$$

$$F_{12} = 212\ d \qquad \text{dynes} \tag{5}$$

in the case of a quartz sphere resting on a plane quartz surface.

2. The macroscopic theory, which is physically more satisfactory, starts from measureable optical properties of the interacting solids and calculates their Van der Waal's attraction from imaginary parts of their complex dielectric constants. According to this theory (ref. 8), the electrons in insulating bodies are subject to random excitations to higher states. This results in spontaneous electrical and magnetic polarization. (The time average of these polarizations is zero.) Using Maxwell's equations, the field strengths associated with these fluctuating polarizations can be written as follows:

$$\text{Curl } E = -\frac{\mu o}{c}\dot{H} \tag{6}$$

$$\text{Curl } H = \frac{1}{c}(\epsilon_o\ \epsilon\ \dot{E} + \dot{K}) \tag{7}$$

where μ_o = induction constant

ϵ_o = influence constant

ϵ = complex dielectric constant

= $\epsilon' + i\ \epsilon''$

and K = electric moment/volume

A Fourier expansion of these field quantities gives a spectral density, $(\overline{E_1\ E_2})_\omega$, of the time average of the electric field strength fluctuations of the following form:

$$\left(\overline{E_1 \ E_2}\right)_\omega = \frac{\hbar}{\pi}\left\{\frac{\omega^2}{\epsilon_o c^2 r} \exp\left(-\frac{\omega r}{c}\sqrt{\frac{|\epsilon| - \epsilon'}{2}}\right) \text{Sin}\left(\frac{\omega r}{c}\sqrt{\frac{|\epsilon| + \epsilon'}{2}}\right)\right.$$

$$\left. + \frac{2\pi\epsilon''}{\epsilon_o |\epsilon|^2}\,\delta(r)\right\} \text{Coth}\,\frac{\hbar\nu}{2kT} \qquad (8)$$

Equation (8) indicates that the Fourier components of the time average field strength fluctuation at different points r_1 and r_2 are correlated over a certain distance, ℓ:

$$\ell = \frac{C}{\omega\sqrt{\left(\frac{|\epsilon| - \epsilon'}{2}\right)}} \qquad (9)$$

$$= \frac{C}{\omega k}$$

when k = complex component of refractive index.

$$\therefore \quad \ell = \frac{2}{K} \qquad (10)$$

$$\because \quad K = \frac{4\pi k}{\lambda}$$

= absorption constant

This equation suggests that Van der Waal's forces result - primarily - from those parts of the electromagnetic spectrum where $K \simeq 10^4\ \text{cm}^{-1}$. Phase correlations of fluctuation fields also occur between two different bodies if they are not too far apart and can lead to bonding if they are not separated by a very dense medium. In the case of two parallel solid surfaces, the Van der Waal's force of attraction per unit area (P) is calculated to be:

$$P = \frac{\hbar\overline{\omega}}{8\pi^2 Z_o^3} \qquad \text{(ref. 7)} \qquad (11)$$

where $$\bar{\omega} = \int_0^{\infty}\left(\frac{\epsilon_1(i\zeta) - 1}{\epsilon_1(i\zeta) + 1}\right)\left(\frac{\epsilon_2(i\zeta) - 1}{\epsilon_2(i\zeta) + 1}\right)d\zeta \qquad (12)^{(*)}$$

where $\bar{\omega} = \omega' + i\zeta$

(i.e., ζ is the imaginary part of the complex angular frequency, ω)

In highly rarefied medium, equation (11) takes the following form:

$$P = \frac{\hbar}{8\pi^2 Z_o^3}\frac{1}{2\pi}\int_0^{\infty}\int_0^{\infty}\frac{\epsilon_1''(\omega_1)\epsilon_2''(\omega_2)}{\omega_1 + \omega_2}d\omega_1 d\omega_2 \qquad (13)$$

Equation (13) is identical to what one would get if we integrate $U(r)$, the interaction potential between two molecules spaced r, over two half spheres separated by Z_o and equate

$$-\frac{dU}{dZ_o} = P$$

In the case of a sphere and a plane surface, the force of attraction becomes:

$$P = \frac{\hbar\bar{\omega}}{8\pi Z_o^2}\frac{d}{2} \qquad (14)$$

Recalling the microscopic theoretic expression for the attractive forces, F (equation (5)),

$$F = \frac{Ad}{24\ Z_o^2} \qquad (15)$$

and noting that $\hbar\,\bar{\omega} = 2\pi/3\ A$, we note that the two expressions are really similar.

Thus in the case of a spherical particle resting on a plane surface in a rarefied medium, the two independent approaches to the calculation of Van der Waal's force lead to the same results.

(*) Indices 1 and 2 in equation (12) represent solids 1 and 2, respectively. The dielectric constant $\epsilon(\omega)$ is treated here as a real function of a complex variable $\omega = \omega' + i\zeta$.

Electrostatic Forces

It is generally recognized that when two neutral bodies are put in contact, there is a transfer of charge from one to the other forming an electrical double layer. In the case of metals, the surface layers carrying such contact charges have a thickness of molecular dimensions, whereas in insulators and semiconductors they may extend as deep as a micrometer. In the case of two semiconductors in contact, the equilibrium contact potential difference, U, is given by:

$$U = \varphi_1 - \varphi_2 \tag{16}$$

where φ_1 and φ_2 represent the electron affinities of the two contacting bodies.

The adhesive force per unit area in the case of two flat surfaces may be written as:

$$P_{el} = \frac{\epsilon_o E^2}{2} = \frac{\epsilon_o U^2}{2 Z_o^2} = \frac{\sigma^2}{2 \epsilon_o} \tag{17}$$

where σ = surface charge density (elementary charges/cm^2)

In general, this approach of calculating P_{el} is not feasible because of imperfect information about the surfaces involved. Krupp (ref. 9) has outlined a model which is applicable to all "technical materials" with a large charge trap density (i.e., high surface state density). According to this model, the contact potential, U, is given by:

$$U = |U_{o1}| + |U_{o2}| \tag{18}$$

where U_{oi} stands for the band bending at the surface of the adherent and the surface charge density, σ_i, is given by:

$$\sigma_i = e\, |U_{oi}| \sqrt{\epsilon_o\, \epsilon\, n_{t\ell}} \tag{19}$$

where $n_{t\ell}$ = trap density per unit energy per unit volume.

In the case of semiconductors (including quartz) the surface charge density, σ_i, ranges from ($10^{11} \rightarrow 10^{13}$)elementary charges/$cm^2$ leading to an electrostatic attractive force, P_{el}, value of less than Van der Waal's attractive force (ref. 9). Accordingly, it appears reasonable to assume that the Van der Waal's pressures predominate in the case of neutral adherents. If, however, the dust particles are strongly charged - as they must be due to collision amongst themselves (ref. 10) - the presence of electrostatic charges will aid the Van der Waal's adhesion force considerably.

APPENDIX 2

PARTICLE ADHESION CRITERION

When dust particles strike against a stationary surface, some of them will rebound and be carried away by the entraining gas stream. Some particles, however, will remain on the surface. The following calculations, which assume the predominance of the Van der Waal's component in adhesive forces, provide some basis for determining which particles will stick to the substrate.

As shown in Appendix 1, the attractive force on a quartz sphere of diameter d centimeters when it is at a distance Z_o of 5 Å from a quartz substrate is given by:

$$F = 212\ d \qquad \text{dynes} \tag{1}$$

The potential energy, P, of the particle at that point is given by:

$$P = -F\ Z_o \tag{2}$$

By imposing conservation of energy and momentum (both linear and angular) it is seen that the incident particle will rebound when its initial vertical velocity component meets the following criterion:

$$V_{\perp}^2 > \frac{2\ P}{m} \left(\frac{1 - e^2}{e^2}\right) \tag{3}$$

where m = particle mass

and e = coefficient of restitution

$\simeq 0.8$ for quartz on quartz

For a particle of density of 2 gm/cc and diameter d microns, equation (3) shows that the incident particle will stick only if

$$V_{\perp} < \frac{30}{d} \qquad \text{centimeters per second} \tag{4}$$

where d is expressed in units of micrometers.

EXPERIMENTAL SET-UP (SCHEMATIC)

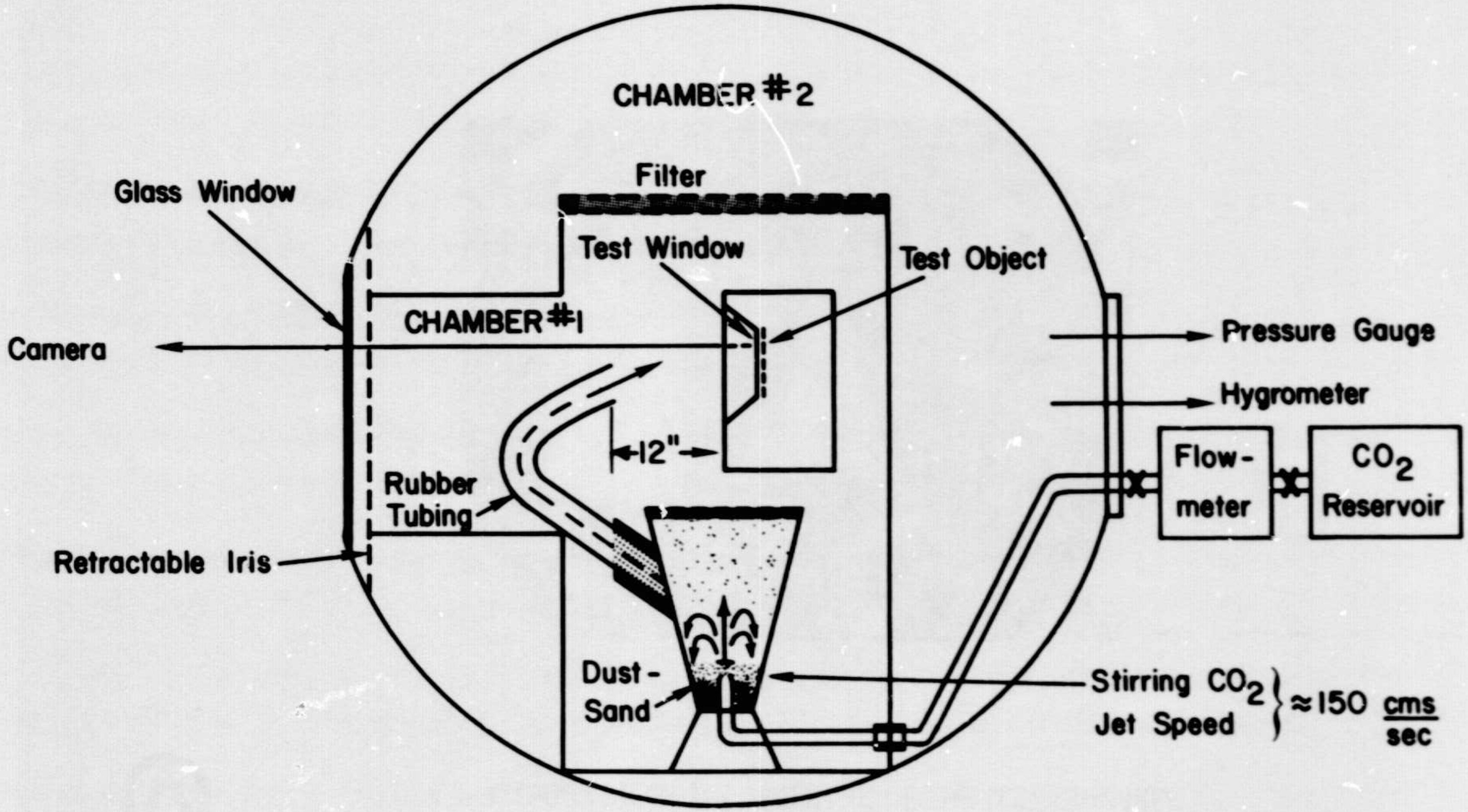

Chamber #1 pumped down by auxiliary pump (50 cfm)

Chamber #2 pumped down by main pump (485 cfm)

Figure-1. - Schematic diagram of the 5'x 5' vacuum chamber used to simulate the Martian atmosphere.

A PHOTOGRAPH OF THE INTERIOR OF THE TEST CHAMBER

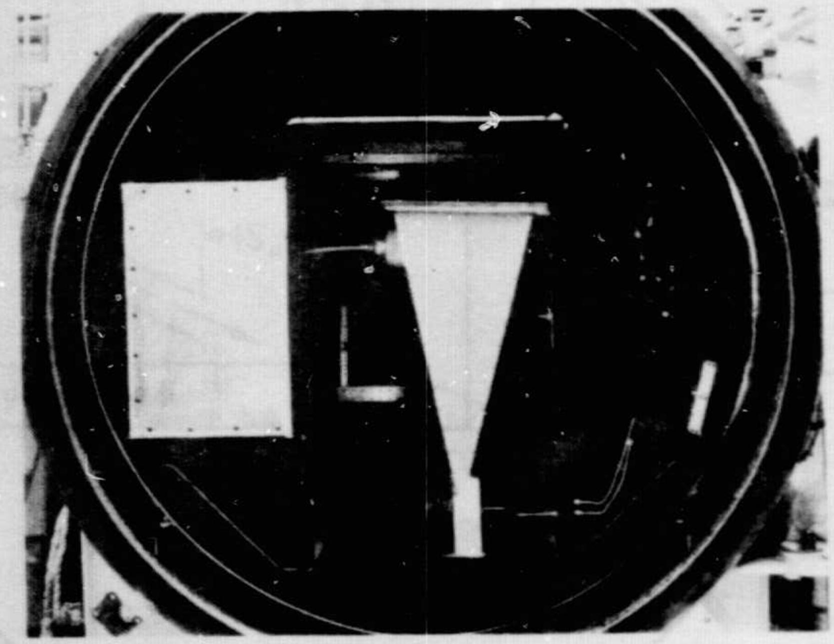

Figure - 2. - Photograph of the interior of the test chamber for the first part of the study.

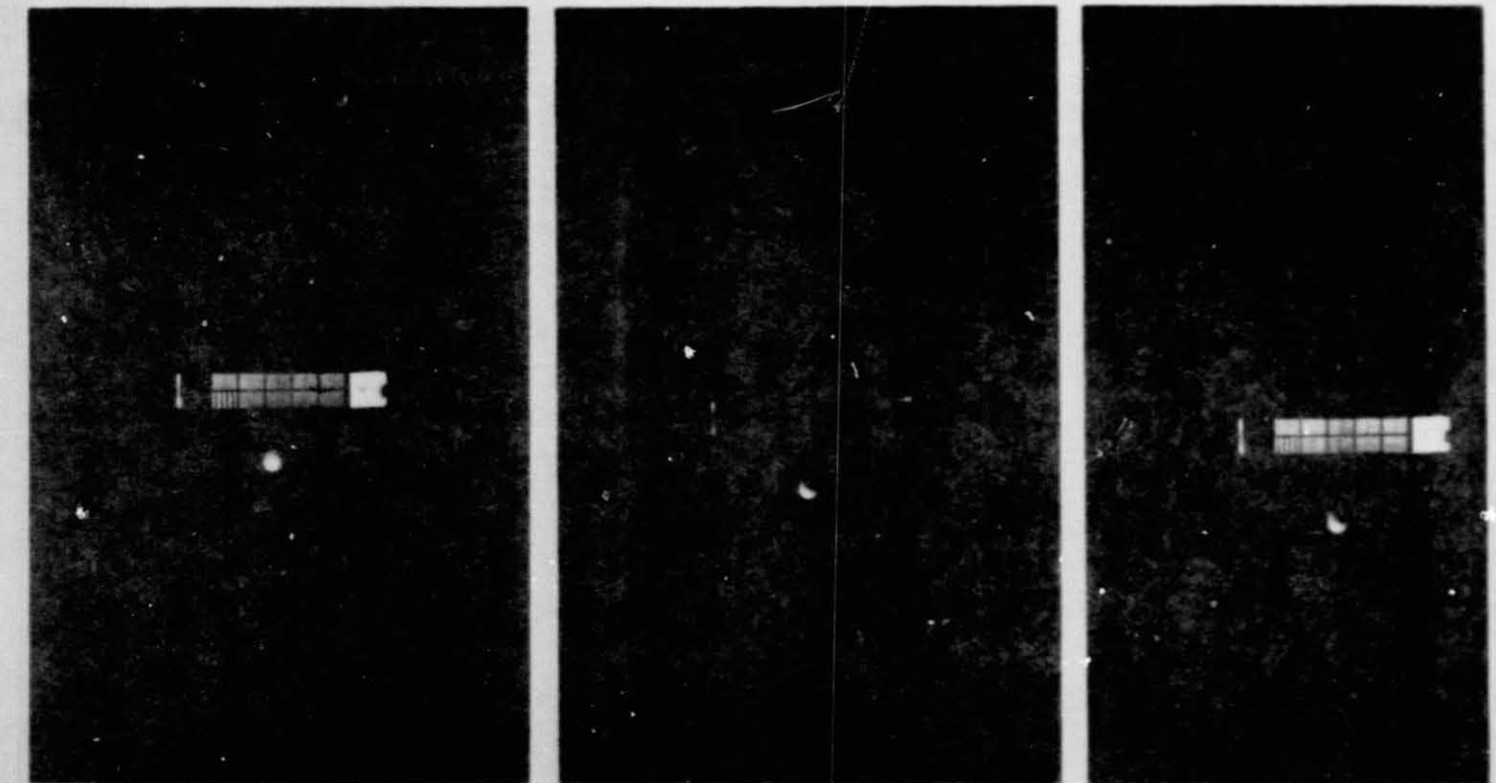

BEFORE AFTER AFTER BLOW-OFF

Figure - 3. - The result of 15 minutes exposure to dust at 1.5 cms / sec.

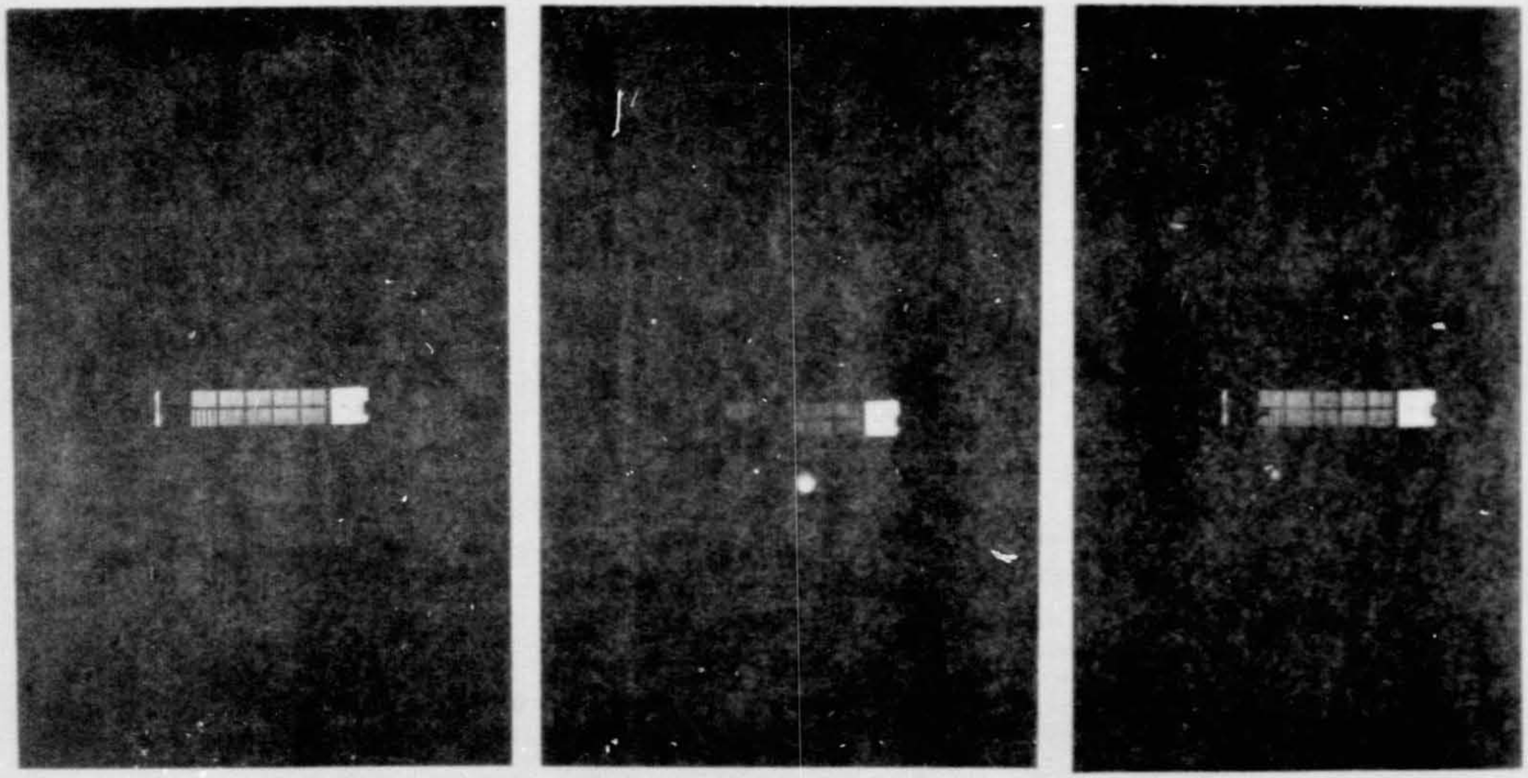

BEFORE AFTER AFTER BLOW-OFF

Figure – 4. – The result of 15 minutes exposure to dust at 15 cms / sec.

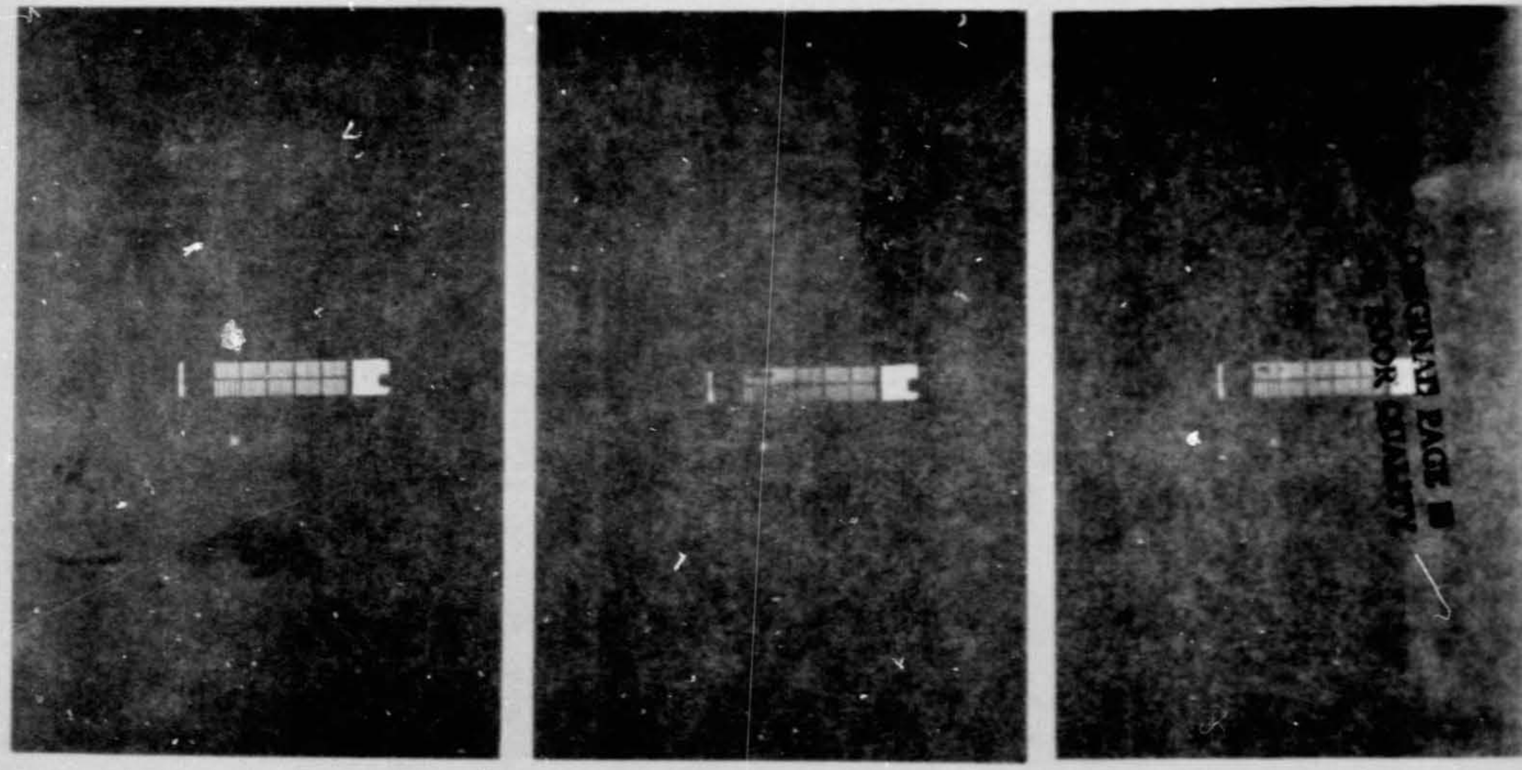

BEFORE | AFTER | AFTER BLOW-OFF

Figure – 5.— The result of 15 minutes exposure to dust at 60 cms / sec.

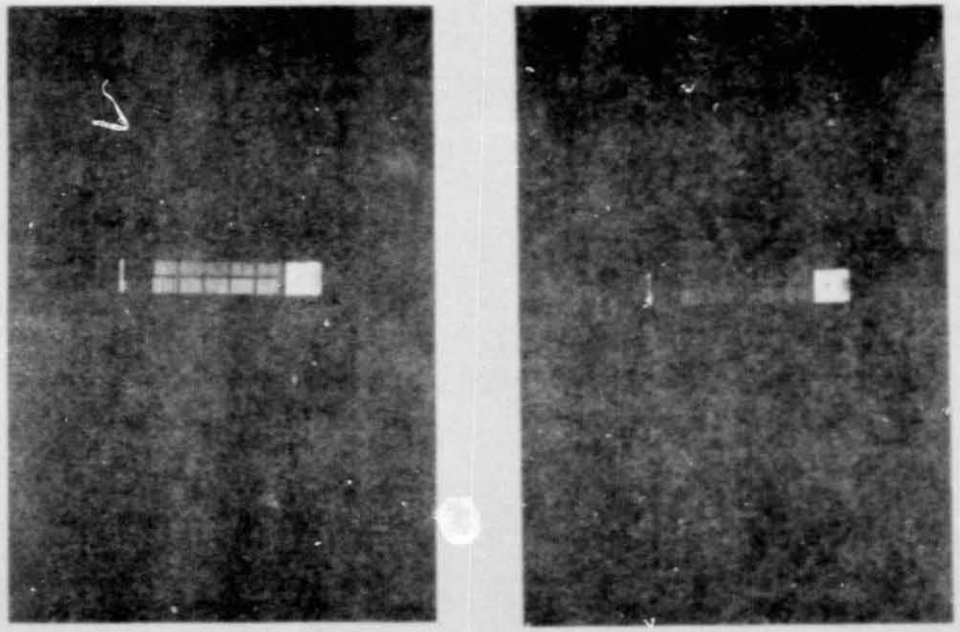

Figure -- 6. – The effect of general dust settlement in the absence of any directed wind. The exposure lasted for 35 minutes.

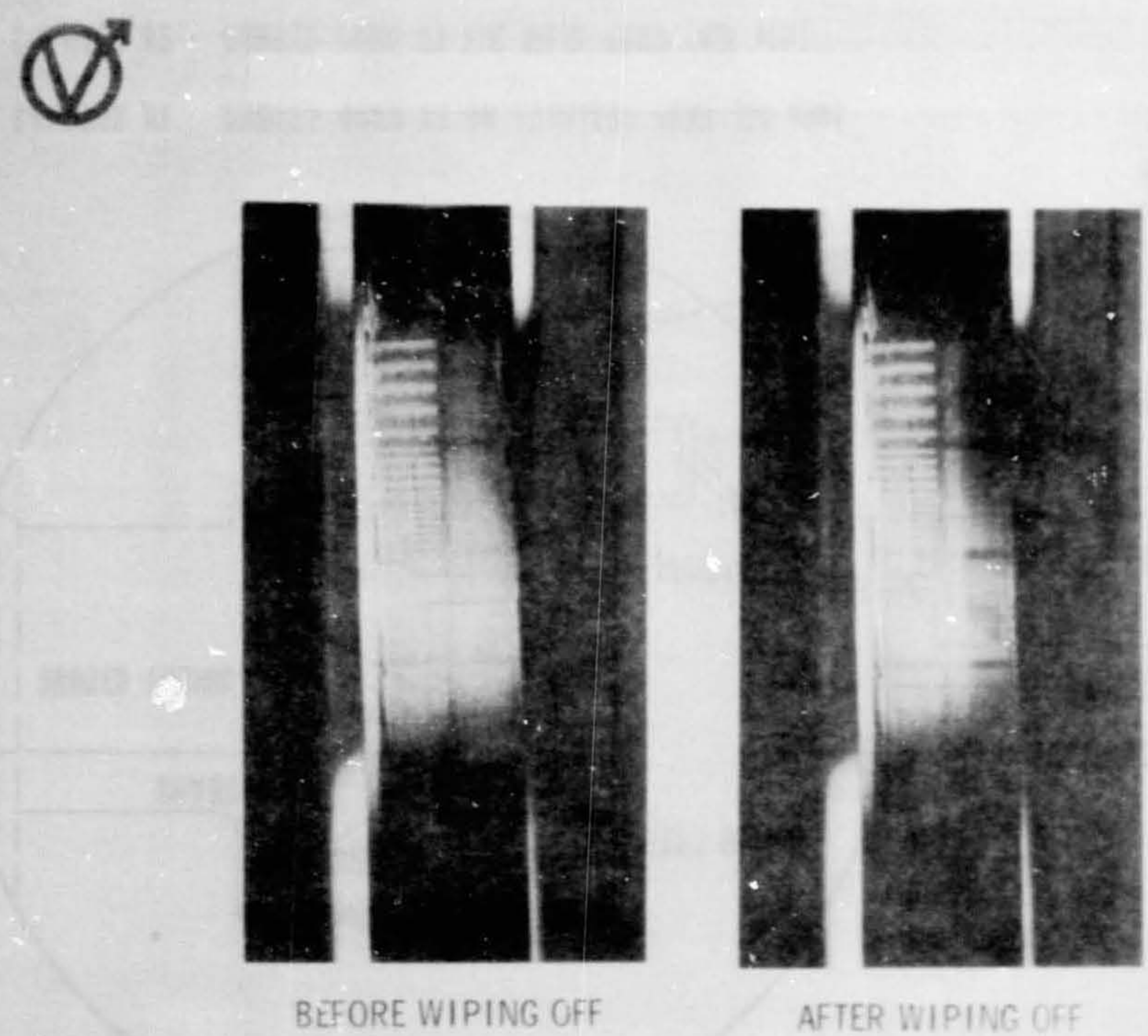

Figure - 7.- An enlarged view of the slide shown in Figure 6.

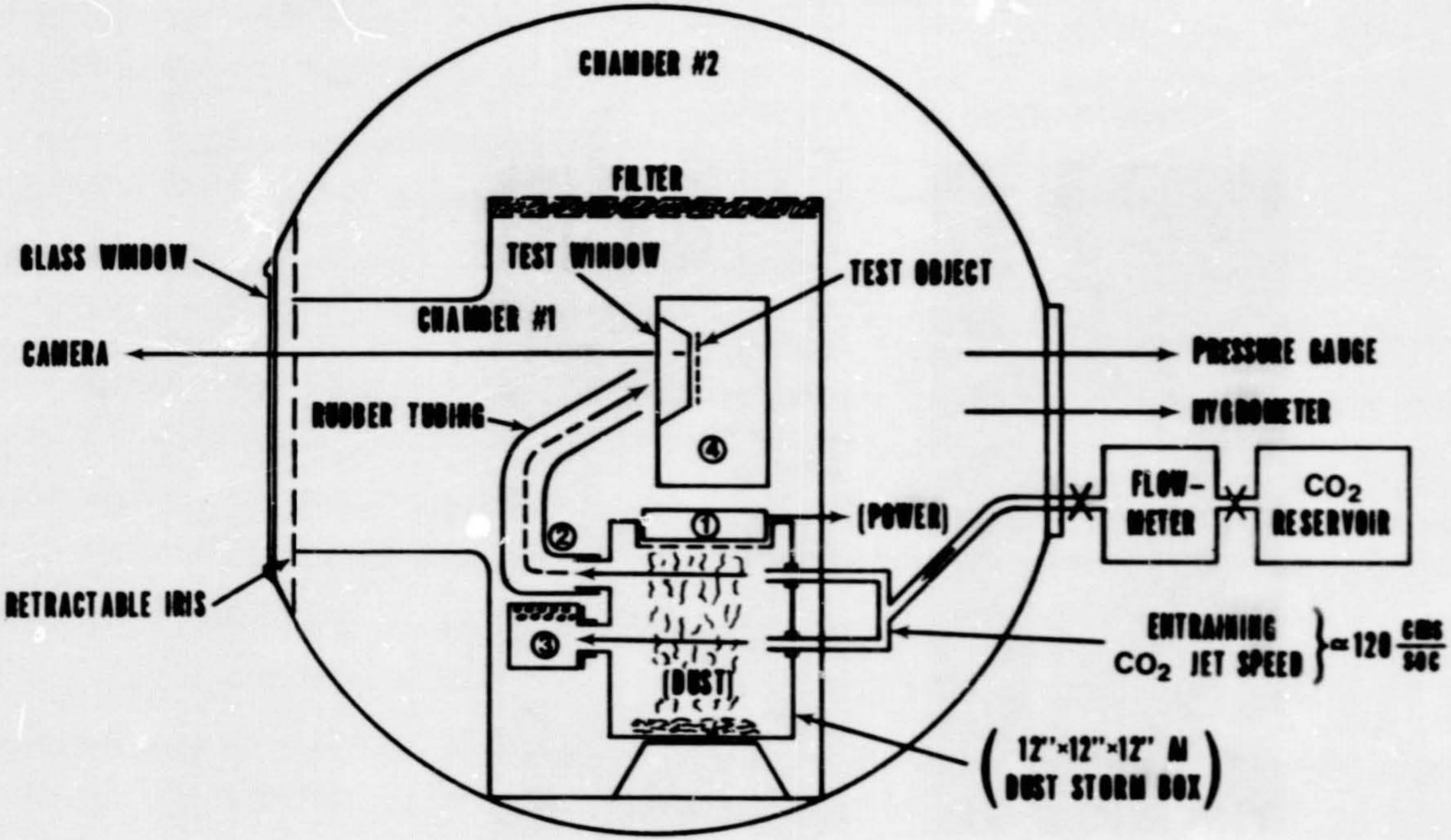

CHAMBER #1 · PUMPED DOWN BY AN AUXILIARY PUMP (50 cfm)

CHAMBER #2 · PUMPED DOWN BY THE MAIN PUMP (465 cfm)

Figure – 8(a).– Schematic diagram of the experimental setup used in the second part of the study.

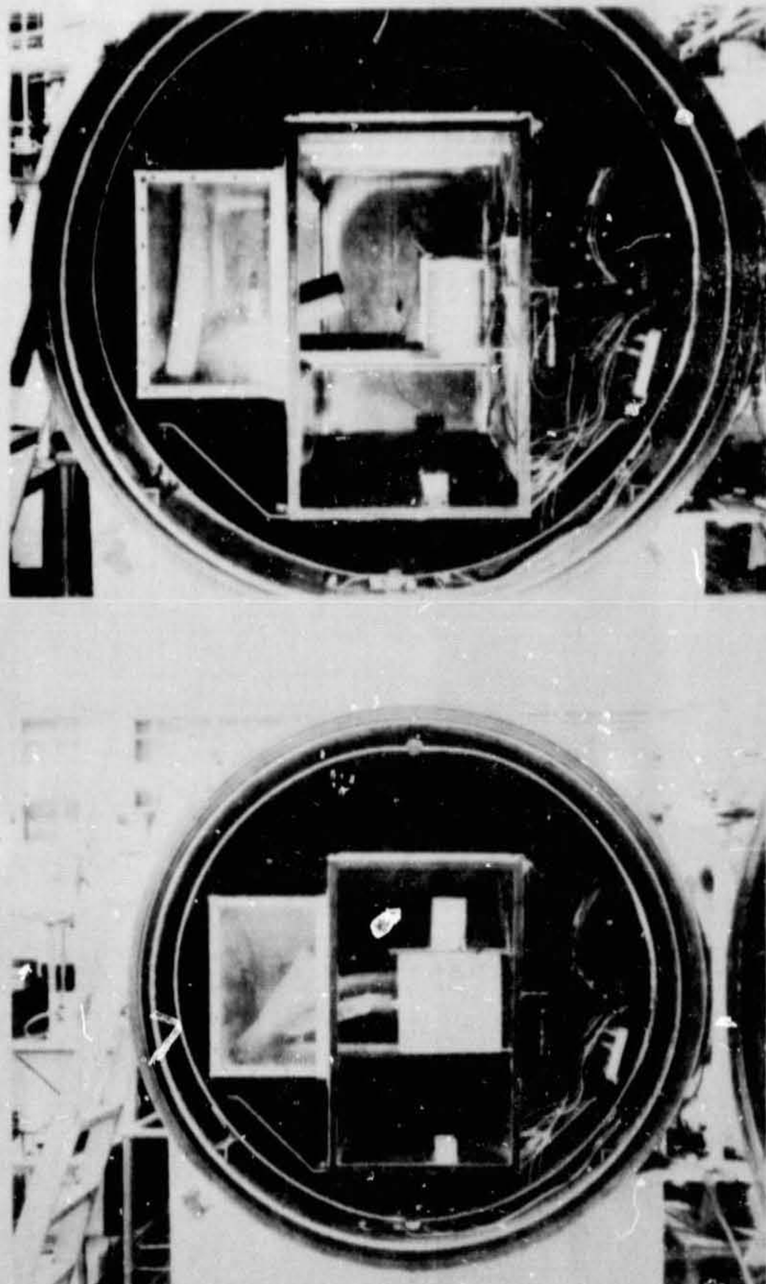

Figure – 8(b) Photographic view of the interior of the test chamber for the second part of the study.

BEFORE DUST | AFTER DUST | AFTER DUST

(135 MINUTES
1.9×10^{-7} GM/CC AT 4 CMS/SEC)

(15 MINUTES
1.6×10^{-6} GM/CC AT 4 CMS/SEC)

FIGURE - 9. A COMPARISON OF DUST ADHESION AT DIFFERENT DUST CONCENTRATIONS FOR ALMOST EQUAL DUST IMPINGEMENT.

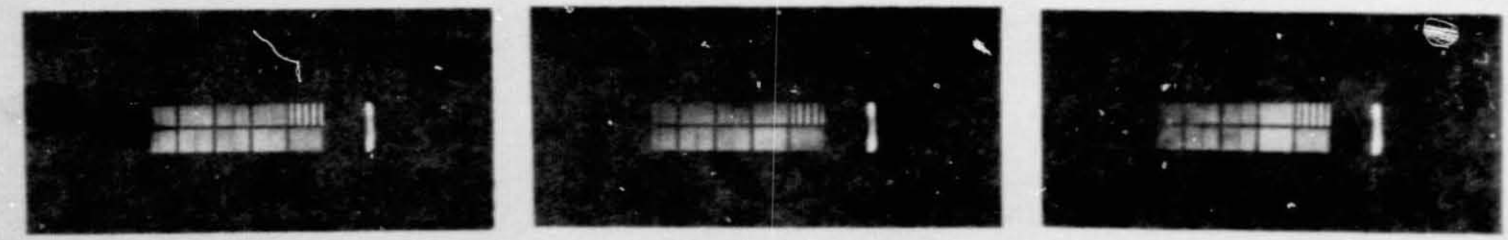

BEFORE DUST

AFTER DUST (60 MINUTES 1.6×10^{-6} GM/CC AT 4 CMS/SEC)

AFTER DUST (15 MINUTES 6.3×10^{-6} GM/CC AT 4 CMS/SEC)

FIGURE -10. A COMPARISON OF DUST ADHESION AT DIFFERENT DUST CONCENTRATIONS FOR EQUAL DUST IMPINGEMENT.

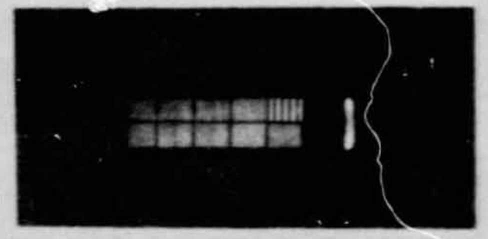

AFTER DUST

(15 MINUTES

6.3×10^{-6} GM/CC AT 4 CMS/SEC

$= 2.52 \times 10^{-5}$ GM/CM^2-SEC)

AFTER DUST

(15 MINUTES

3×10^{-6} GM/CC AT 8 CMS/SEC

$= 2.4 \times 10^{-5}$ GM/CM^2-SEC)

FIGURE -11. COMPARISON OF DUST ADHESION AT DIFFERENT CONCENTRATIONS AND SPEEDS FOR ALMOST EQUAL DUST IMPINGEMENT.

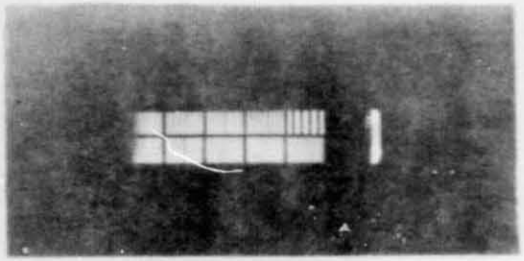

BEFORE DUST

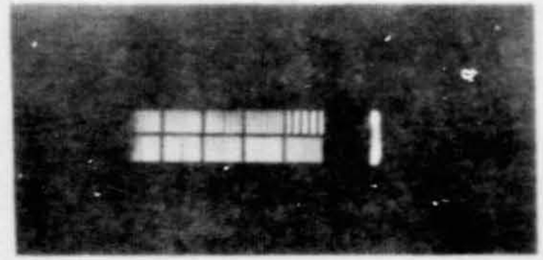

AFTER DUST

(15 MINUTES

4.5×10^{-6} GM/CC AT 4 CMS/SEC)

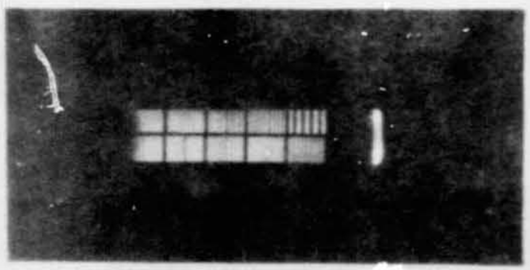

AFTER DUST

(30 MINUTES

4.5×10^{-6} GM/CC AT 4 CMS/SEC)

AFTER DUST

60 MINUTES

4.5×10^{-6} GM/CC AT 4 CMS/SEC)

FIGURE -12. DUST BUILD-UP AS A FUNCTION OF EXPOSURE TIME AT A CONSTANT SPEED AND CONCENTRATION.

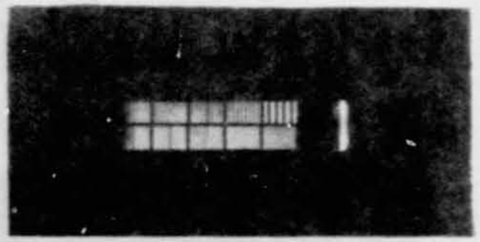

BEFORE DUST

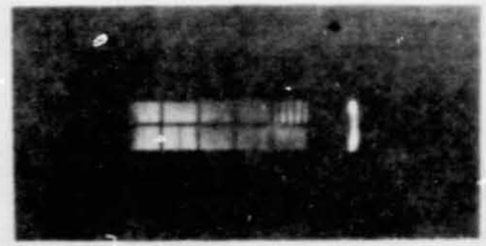

AFTER DUST

(60 MINUTES

4.5×10^{-6} GM/CC AT 4 CMS/SEC)

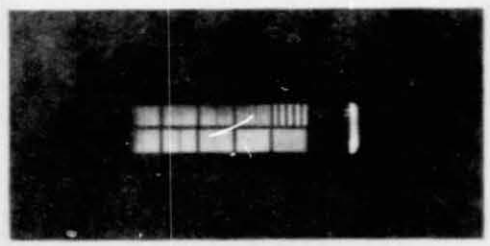

AFTER BLOW-OFF

0.1 SEC CO_2

JET AT 1000 PSI

FIGURE -13. THE EFFECTIVENESS OF A SINGLE CO_2 JET (0.1 SEC/1000 PSI) IN CLEARING UP THE DUST COVERED WINDOW